Acta Cryst E CRYSTALLOGRAPHIC COMMUNICATIONS

ISSN 2056-9890

Crystal structure of bis{3-(3,5-dichlorophenyl)-5-[6-(1*H*-pyrazol-1-yl)pyridin-2-yl]-4*H*-1,2,4-triazol-4-ido}iron(II) methanol disolvate

Kateryna Znovjyak,[a]* Maksym Seredyuk,[a] Igor O. Fritsky,[a] Tatiana Y. Sliva,[a] Vladimir M. Amirkhanov,[a] Sergey O. Malinkin[a] and Sergiu Shova[b]

[a]Department of Chemistry, Taras Shevchenko National University of Kyiv, Volodymyrska Street 64, Kyiv, 01601, Ukraine, and [b]Department of Inorganic Polymers, "Petru Poni" Institute of Macromolecular Chemistry, Romanian Academy of Science, Aleea Grigore Ghica Voda 41-A, Iasi 700487, Romania. *Correspondence e-mail: znovkat@yahoo.com

Received 26 September 2022
Accepted 31 October 2022

Edited by J. Ellena, Universidade de São Paulo, Brazil

Keywords: crystal structure; iron(II) complexes; neutral complexes.

CCDC reference: 2216680

Supporting information: this article has supporting information at journals.iucr.org/e

The asymmetric unit of the title compound, $[Fe^{II}(C_{16}H_9Cl_2N_6)_2]\cdot 2CH_3OH$, consists of half of a charge-neutral complex molecule and a discrete methanol molecule. The planar anionic tridentate ligand 2-[5-(3,5-dichlorophenyl)-4*H*-1,2,4-triazol-3-ato]-6-(1*H*-pyrazol-1-yl)pyridine coordinates to the Fe^{II} ion through the N atoms of the pyrazole, pyridine and triazole groups, forming a coordination sphere of the central ion that deviates moderately from an octahedral geometry. The average Fe—N bond distance is 1.953 Å, indicating the low-spin state of the Fe^{II} ion. The cone-like-shaped molecules, nested into each other, are linked through double weak C—H(pz)···π(ph) interactions into mono-periodic columns, which are further linked through weak C—H···N′/C′ interactions into di-periodic layers. The layers interact through double weak C–H(ph)···Cl bonds with neighbouring molecules. Energy framework analysis at the B3LYP/6–31 G(d,p) theory level reproduces the strong interaction within the layers and the weaker interlayer interactions. Intermolecular contacts were quantified using Hirshfeld surface analysis and two-dimensional fingerprint plots, the relative contributions of the contacts to the crystal packing being H···H 26.1%, H···C/C···H 24.4%, H···Cl/Cl···H 18.9% and H···N/N···H 12.1%.

1. Chemical context

Meridional tridentate ligands, to which different bisazolepyridines belong, are a common choice for the synthesis of Fe^{II} spin-crossover compounds able to switch between a high-spin state ($t_{2g}^4e_g^2$, total spin S = 2) and the low-spin state ($t_{2g}^6e_g^0$, total spin S = 0) due to temperature change, irradiation or external pressure (Goodwin, 2004; Halcrow *et al.*, 2019). In the case of asymmetric ligands with one of the azole groups carrying a hydrogen on the nitrogen heteroatom, deprotonation can produce neutral $[Fe(ligand)_2]$ complexes that can be high-spin (Schäfer *et al.*, 2013), low-spin (Shiga *et al.*, 2019) or spin crossover (Seredyuk *et al.*, 2014), depending on the constituent organic groups, solvent molecules and the way that the molecules interact in the lattice (Seredyuk *et al.*, 2022).

Having an interest in Fe^{II} spin-crossover complexes formed by polydentate ligands (Bonhommeau *et al.*, 2012; Valverde-Muñoz *et al.*, 2020; Piñeiro-López *et al.*, 2021), we report here on a structural characterization of a new complex $[Fe^{II}L_2]^0$ based on asymmetric deprotonable ligand L = 2-[5-(3,5-dichlorophenyl)-4*H*-1,2,4-triazol-3-yl]-6-(1*H*-pyrazol-1-yl)pyridine.

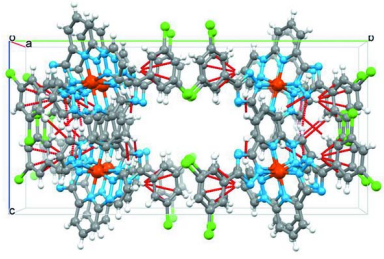

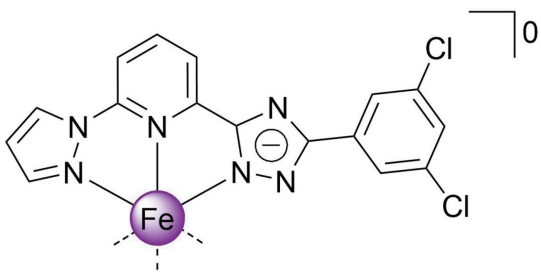

2. Structural commentary

The asymmetric unit comprises half of the molecule and a discrete MeOH molecule forming an O26—H26···N16 hydrogen bond with the triazole (trz) ring and a weak C5—H5···O26 bond with the pyridine (py) ring (Fig. 1). The Fe^{II} ion has a pseudo-octahedral coordination environment composed of the nitrogen donor atoms of the pyrazole (pz), py, and trz heterocycles with an averaged <Fe—N> distance of 1.953 Å (V[FeN_6] = 9.610 $Å^3$) that is typical for low-spin complexes with an N_6 coordination environment (Gütlich & Goodwin, 2004). The pz, py, trz, and phenyl rings of the ligand lie essentially in the same plane (r.m.s.deviation = 0.156 Å).

The average trigonal distortion parameters $\Sigma = \Sigma_1^{12}(|90 - \varphi_i|)$, where φ_i is the N—Fe—N′ angle (Drew *et al.*, 1995), and $\Theta = \Sigma_1^{24}(|60 - \theta_i|)$, where θ_i is the angle generated by the superposition of two opposite faces of the octahedron (Chang *et al.*, 1990), are 91.2 and 291.5°, respectively. The values reveal a deviation of the coordination environment from an ideal octahedron in the expected range for complexes with similar bisazolepyridine ligands (see below). The calculated continuous shape measure [CShM(O_h)] value relative to the ideal octahedral symmetry is 2.16 (Kershaw Cook *et al.*, 2015).

3. Supramolecular features

As a result of their tapered shape, neighbouring complex molecules are embedded in each other and interact through two weak intermolecular C—H(pz)···π(ph^{i}) contacts between

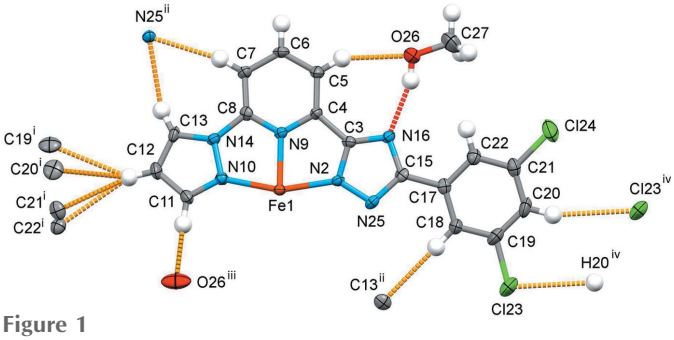

Figure 1
The molecular structure of half of the title compound with displacement ellipsoids drawn at the 50% probability level. The strong O—H···N and weak C—H···O/N/C/Cl hydrogen bonds are shown with the nearest neighbours. Symmetry codes: (i) $-1+x, \frac{1}{2}-y, \frac{1}{2}-z$; (ii) $-\frac{1}{2}+x, \frac{1}{2}-y, \frac{1}{2}+z$; (iii) $-\frac{1}{2}+x, \frac{1}{2}-y, -\frac{1}{2}+z$; (iv) $2-x, 1-y, -z$.

Table 1
Hydrogen-bond geometry (Å, °).

D—H···A	D—H	H···A	D···A	D—H···A
C5—H5···O26	0.95	2.41	3.256 (6)	149
C7—H7···N25^{i}	0.95	2.48	3.406 (5)	165
C11—H11···O26^{ii}	0.95	2.23	3.144 (6)	162
C13—H13···N25^{i}	0.95	2.52	3.363 (6)	148
C20—H20···Cl23^{iii}	0.95	2.86	3.779 (5)	162
O26—H26···N16	0.88 (5)	1.96 (5)	2.826 (5)	166 (5)

Symmetry codes: (i) $x-\frac{1}{2}, -y+\frac{1}{2}, z+\frac{1}{2}$; (ii) $x-\frac{1}{2}, -y+\frac{1}{2}, z-\frac{1}{2}$; (iii) $-x+2, -y+1, -z$.

the pyrazole (pz) and phenyl (ph) groups [the C(12)(pz)···C_g(ph^{i}) distance is 3.458 Å and the angle between the ring planes is 80.0°; symmetry code: (i) $-1+x, \frac{1}{2}-y, \frac{1}{2}-z$]. The formed one-dimensional supramolecular columns protrude along the *a*-axis with a stacking periodicity equal to 10.4669 (6) Å (= cell parameter *a*) (Fig. 2*a*). As a result of weak intermolecular C—H(pz,py)···N/C(pz,trz)/O(MeOH) hydrogen bonds in the range 2.826 (5)–3.779 (5) Å (Table 1), neighbouring columns are joined into corrugated di-periodic layers in the *ac* plane (Fig. 2*b*,*c*). The layers stack along the *b*-axis direction, forming weak C—H(ph)···Cl(ph^{ii}) [symmetry code: (ii) $2-x, 1-y, -z$] interlayer interactions shorter than the sum of the van der Waals radii, two per each phenyl group (Fig. 2*c*). The voids between the layers are occupied by methanol molecules, which participate in the strong and weak hydrogen bonding mentioned above. A complete list of intermolecular interactions is given in Table 1.

4. Hirshfeld surface and 2D fingerprint plots

A Hirshfeld surface analysis was performed and the associated two-dimensional fingerprint plots were generated using *Crystal Explorer* (Spackman *et al.*, 2021), with a standard resolution of the three-dimensional d_{norm} surfaces plotted over a fixed colour scale of −0.5982 (red) to 1.2057 (blue) a.u.

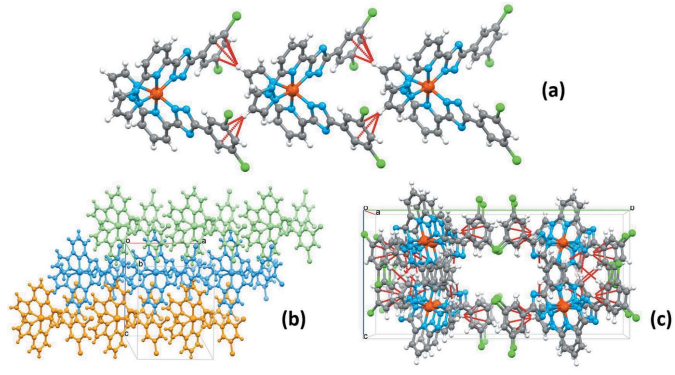

Figure 2
(*a*) A fragment of mono-periodic supramolecular column formed by stacking of molecules along the *a* axis; (*b*) supramolecular di-periodic layers formed by stacking of the supramolecular columns in the *ac* plane. For a better representation, each column has a different colour; (*c*) stacking of the di-periodic layers along the *b* axis. The methanol molecules are not shown for clarity.

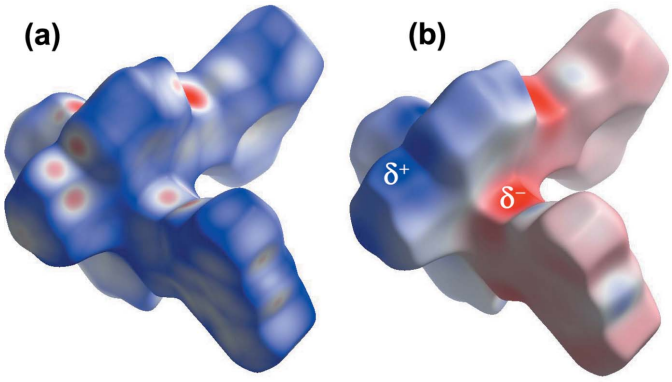

Figure 3
(*a*) A projection of d_{norm} mapped on Hirshfeld surfaces, showing the intermolecular interactions within the molecule. Red/blue and white areas represent regions where contacts are shorter/larger than the sum and close to the sum of the van der Waals radii, respectively. (*b*) Electrostatic potential for the title compound derived from a B3LYP/6–31 G(d,p) wavefunction mapped on the Hirshfeld surface in the range −0.1043 (red) to 0.1064 a.u. (blue).

(Fig. 3*a*). The pale-red spots indicate short contacts and negative d_{norm} values on the surface correspond to the interactions described above. The overall two-dimensional fingerprint plot is illustrated in Fig. 4. The Hirshfeld surfaces mapped over d_{norm} are shown for the H···H, H···C/C···H, H···Cl/Cl···H and H···N/N···H contacts, and the two-dimensional fingerprint plots, associated with their relative contributions to the Hirshfeld surface. At 26.1%, the largest contribution to the overall crystal packing is from H···H interactions, which are located mostly in the middle region of the fingerprint plot. H···C/C···H contacts contribute 24.4% and H···Cl/Cl···H 18.9%, resulting in a pair of characteristic wings. The H···N/N···H contacts, represented by a pair of sharp spikes in the fingerprint plot, make a 12.1% contribution to the Hirshfeld surface. The electrostatic potential energy calculated using the B3LYP/6-31G(d,p) basis set localizes the negative charge on the trz-ph moieties of the complex molecule, while the pz-py moieties are relatively positively charged (Fig. 3*b*). The polar nature of the molecule justifies the realized stacking in columns.

5. Energy framework analysis

The energy framework (Spackman *et al.*, 2021) with total energy values (E_{tot}) calculated using the wavefunction at the B3LYP/6-31G(d,p) theory level are shown in Fig. 5*a*. The cylindrical radii are proportional to the relative strength of the corresponding energies. The major contribution to the intermolecular interactions comes from dispersion forces (E_{dis}), reflecting the dominant type of interactions in the network of the electroneutral molecules (see the table in Fig. 5). The energy framework topology reproduces the topology of intermolecular interactions within and between supramolecular layers, including the electron-density distribution within the molecule analysed above using mapped Hirshfeld surfaces. The weak hydrogen bonding between the molecules

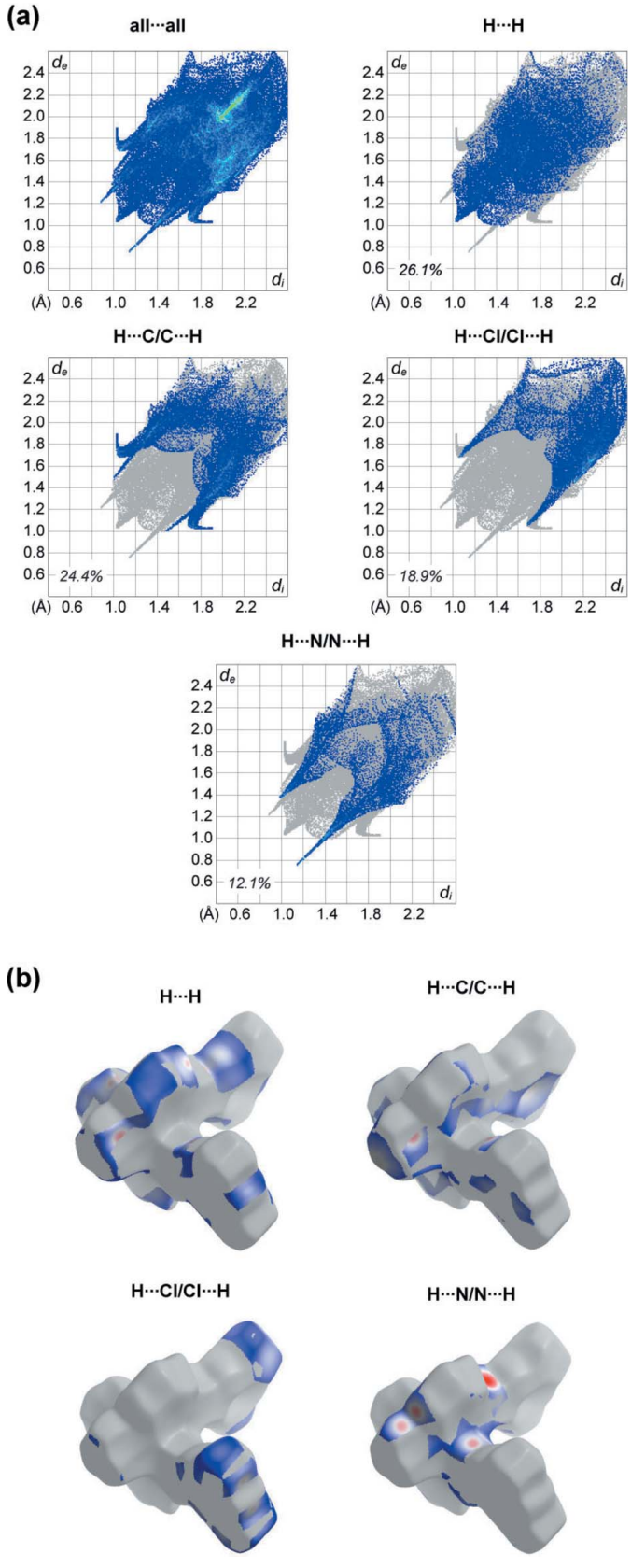

Figure 4
(*a*) The overall two-dimensional fingerprint plot and those delineated into specified interactions. (*b*) Hirshfeld surface representations with the function d_{norm} plotted onto the surface for the different interactions.

Table 2
Computed distortion indices (Å, °) for the title compound and similar complexes from the literature.

CSD refcode	Spin state	<Fe—N>	Σ	Θ	CShM(O_h)
Title compound	Low-spin	1.953	91.2	291.5	2.16
XODCEB[a]	Low-spin	1.950	87.4	276.6	1.92
IGERIX[b]	High-spin	2.179	149.7	553.2	6.06
IGERIX01[b]	Low-spin	1.986	105.6	350.6	2.85
LUTGEO[c]	Low-spin	1.933	85.0	309.6	2.10

Notes: (*a*) Shiga *et al.* (2019); (*b*) Gentili *et al.* (2015); (*c*) Senthil Kumar *et al.* (2015).

within the supramolecular columns and between the columns within the layers correspond to interaction energies of −48.6 and −67.9 kJ mol^{-1}, respectively (Fig. 5*b*). As for the interlayer interactions, the double supramolecular C—H···Cl^{ii} [symmetry code: (ii) 2 − *x*, 1 − *y*, −*z*] bonding between neighbouring phenyl rings leads to an interaction energy of −5.6 kJ mol^{-1}, while the stacking of the moieties corresponds to an interaction energy of −21.7 kJ mol^{-1} (Fig. 5*c*). The colour-coded interaction mappings within a radius of 3.8 Å of a central reference molecule for the title compound together with full details of the various contributions to the total energy (E_{ele}, E_{pol}, E_{dis}, E_{rep}) are shown in the table in Fig. 5.

6. Database survey

A search of the Cambridge Structural Database (CSD, Version 5.42, last update February 2021; Groom *et al.*, 2016) reveals similar neutral Fe^{II} complexes with a deprotonable azole based on pyrazole-pyridine-benzimidazole, *viz*. XODCEB (Shiga *et al.*, 2019) and pyrazole-pyridine-tetrazole, IGERIX and LUTGEO (Gentili *et al.*, 2015; Senthil Kumar *et al.*, 2015). The Fe—N distances for these complexes in the low-spin state are close to the value in the title compound, while in the high-spin state it is larger by ∼0.2 Å. The trigonal distortion indices change correspondingly, and in the low-spin state they are systematically lower than in the high-spin state. Table 2 collates the structural parameters of the complexes and of the title compound.

7. Synthesis and crystallization

The synthesis of the title compound was performed using a layering technique in a standard test tube. The layering sequence was as follows: the bottom layer contains a solution of [Fe(L_2)](BF_4)$_2$ prepared by dissolving *L* = [2-(3,5-dichlorophenyl)-4*H*-1,2,4-triazol-3-yl]-6-(1*H*-pyrazol-1-yl)pyridine (100 mg, 0.280 mmol) and Fe(BF_4)$_2$·6H_2O (47 mg, 0.140 mmol) in boiling acetone, to which chloroform (5 ml) was then added. The middle layer was a methanol–chloroform mixture (1:10, 10 ml), which was covered by a layer of methanol (10 ml), to which 100 µl of NEt_3 was added dropwise. The tube was sealed, and thin lustrous black plate-like single crystals appeared in 3–4 weeks (yield *ca* 60%). Elemental analysis calculated for $C_{34}H_{26}Cl_4FeN_{12}O_2$: C, 49.06; H, 3.15; N, 20.19. Found: C, 49.24; H, 3.05; N, 20.10.

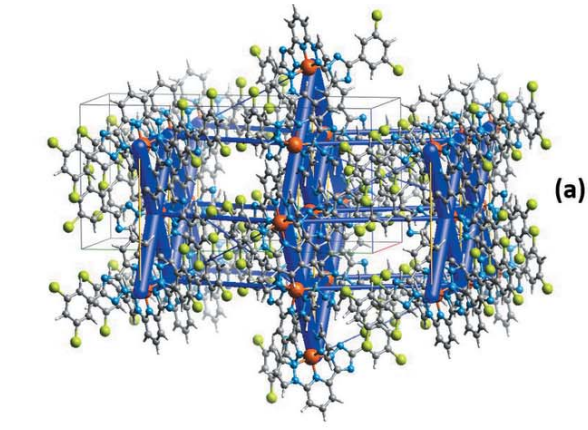

	Symmetry operation	R, Å	E_{ele}	E_{pol}	E_{dis}	E_{rep}	E_{tot}
	x+1/2, y, -z	8.28	-24.1	-16.5	-85.5	71.6	-67.9
	x, y, z	10.47	-25.1	-6.4	-42.4	31.7	-48.6
	-x+1/2, -y, z	14.00	0.4	-3.0	-40.1	24.3	-21.7
	x, y, z	12.84	12.9	-1.9	-6.2	0.8	7.4
	-x, -y, -z	17.62	-5.6	-0.9	-14.1	21.5	-5.6

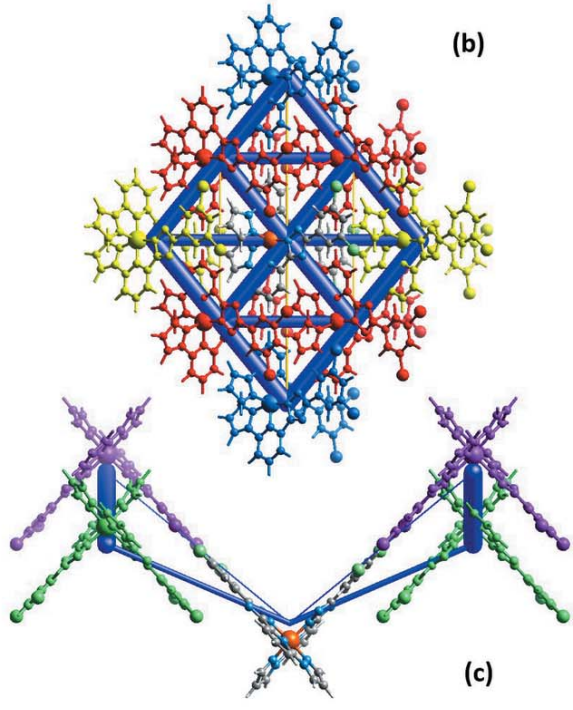

Figure 5
(*a*) The calculated energy frameworks, showing the total energy diagrams (E_{tot}), (*b*) decomposition of the energy framework into the part corresponding to the interactions within a supramolecular layer and (*c*) interlayer interactions. In the table the corresponding colour-coded energy values E_{tot} are provided, including their E_{ele}, E_{pol}, E_{dis}, and E_{rep} components. Tube size is set at 100 scale, the blue colour corresponds to the attractive interaction, yellow to the repulsive interaction.

8. Refinement details

Crystal data, data collection and structure refinement details are summarized in Table 3. H atoms were placed in calculated positions using idealized geometries, with C—H = 0.98 Å for methyl groups and 0.95 Å for aromatic H atoms, and refined using a riding model with U_{iso}(H) = 1.2–1.5U_{eq}(C); the hydrogen atom H26 was refined freely.

Acknowledgements

Author contributions are as follows: Conceptualization, KZ and MS; methodology, KZ; formal analysis, IOF; synthesis, SOM; single-crystal measurements, SS; writing (original draft), MS; writing (review and editing of the manuscript), TYS, MS; visualization and calculations, VMA; funding acquisition, KZ, MS.

Funding information

Funding for this research was provided by a grant from the Ministry of Education and Science of Ukraine for perspective development of the scientific direction 'Mathematical sciences and natural sciences' at Taras Shevchenko National University of Kyiv and by the Ministry of Education and Science of Ukraine (grant Nos. 22BF037-03, 22BF037-04).

Table 3
Experimental details.

Crystal data	
Chemical formula	$[Fe(C_{16}H_9Cl_2N_6)_2]\cdot 2CH_4O$
M_r	832.32
Crystal system, space group	Orthorhombic, *Pnna*
Temperature (K)	180
a, *b*, *c* (Å)	10.4669 (6), 26.5890 (16), 12.8313 (7)
V (Å^3)	3571.0 (4)
Z	4
Radiation type	Mo *Kα*
μ (mm^{-1})	0.77
Crystal size (mm)	0.12 × 0.08 × 0.03
Data collection	
Diffractometer	Xcalibur, Eos
Absorption correction	Multi-scan (*CrysAlis PRO*; Rigaku OD, 2022)
T_{min}, T_{max}	0.772, 1.000
No. of measured, independent and observed [$I > 2\sigma(I)$] reflections	13877, 3650, 2093
R_{int}	0.100
(sin $\theta/\lambda)_{max}$ (Å^{-1})	0.625
Refinement	
$R[F^2 > 2\sigma(F^2)]$, $wR(F^2)$, *S*	0.068, 0.133, 1.02
No. of reflections	3650
No. of parameters	244
H-atom treatment	H atoms treated by a mixture of independent and constrained refinement
$\Delta\rho_{max}$, $\Delta\rho_{min}$ (e Å^{-3})	0.44, −0.50

Computer programs: *CrysAlis PRO* (Rigaku OD, 2022), *SHELXL2018/3* (Sheldrick, 2015) and *OLEX2* (Dolomanov *et al.*, 2009).

References

Bonhommeau, S., Lacroix, P. G., Talaga, D., Bousseksou, A., Seredyuk, M., Fritsky, I. O. & Rodriguez, V. (2012). *J. Phys. Chem. C*, **116**, 11251–11255.

Chang, H. R., McCusker, J. K., Toftlund, H., Wilson, S. R., Trautwein, A. X., Winkler, H. & Hendrickson, D. N. (1990). *J. Am. Chem. Soc.* **112**, 6814–6827.

Dolomanov, O. V., Bourhis, L. J., Gildea, R. J., Howard, J. A. K. & Puschmann, H. (2009). *J. Appl. Cryst.* **42**, 339–341.

Drew, M. G. B., Harding, C. J., McKee, V., Morgan, G. G. & Nelson, J. (1995). *J. Chem. Soc. Chem. Commun.* pp. 1035–1038.

Gentili, D., Demitri, N., Schäfer, B., Liscio, F., Bergenti, I., Ruani, G., Ruben, M. & Cavallini, M. (2015). *J. Mater. Chem. C.* **3**, 7836–7844.

Goodwin, H. A. (2004). *Top. Curr. Chem.* **233**, 59–90.

Groom, C. R., Bruno, I. J., Lightfoot, M. P. & Ward, S. C. (2016). *Acta Cryst.* B**72**, 171–179.

Gütlich, P. & Goodwin, H. A. (2004). *Top. Curr. Chem.* **233**, 1–47.

Halcrow, M. A., Capel Berdiell, I., Pask, C. M. & Kulmaczewski, R. (2019). *Inorg. Chem.* **58**, 9811–9821.

Kershaw Cook, L. J., Mohammed, R., Sherborne, G., Roberts, T. D., Alvarez, S. & Halcrow, M. A. (2015). *Coord. Chem. Rev.* **289–290**, 2–12.

Piñeiro-López, L., Valverde-Muñoz, F.-J., Trzop, E., Muñoz, M. C., Seredyuk, M., Castells-Gil, J., da Silva, I., Martí-Gastaldo, C., Collet, E. & Real, J. A. (2021). *Chem. Sci.* **12**, 1317–1326.

Rigaku OD (2022). *CrysAlis PRO*. Rigaku Oxford Diffraction, Yarnton, England.

Schäfer, B., Rajnák, C., Šalitroš, I., Fuhr, O., Klar, D., Schmitz-Antoniak, C., Weschke, E., Wende, H. & Ruben, M. (2013). *Chem. Commun.* **49**, 10986–10988.

Senthil Kumar, K., Šalitroš, I., Heinrich, B., Fuhr, O. & Ruben, M. (2015). *J. Mater. Chem. C.* **3**, 11635–11644.

Seredyuk, M., Znovjyak, K., Valverde-Muñoz, F. J., da Silva, I., Muñoz, M. C., Moroz, Y. S. & Real, J. A. (2022). *J. Am. Chem. Soc.* **144**, 14297–14309.

Seredyuk, M., Znovjyak, K. O., Kusz, J., Nowak, M., Muñoz, M. C. & Real, J. A. (2014). *Dalton Trans.* **43**, 16387–16394.

Sheldrick, G. M. (2015). *Acta Cryst.* C**71**, 3–8.

Shiga, T., Saiki, R., Akiyama, L., Kumai, R., Natke, D., Renz, F., Cameron, J. M., Newton, G. N. & Oshio, H. (2019). *Angew. Chem. Int. Ed.* **58**, 5658–5662.

Spackman, P. R., Turner, M. J., McKinnon, J. J., Wolff, S. K., Grimwood, D. J., Jayatilaka, D. & Spackman, M. A. (2021). *J. Appl. Cryst.* **54**, 1006–1011.

Valverde-Muñoz, F.-J., Seredyuk, M., Muñoz, M. C., Molnár, G., Bibik, Y. S. & Real, J. A. (2020). *Angew. Chem. Int. Ed.* **59**, 18632–18638.

supporting information

Acta Cryst. (2022). E**78**, 1173-1177 [https://doi.org/10.1107/S2056989022010507]

Crystal structure of bis{3-(3,5-dichlorophenyl)-5-[6-(1*H*-pyrazol-1-yl)pyridin-2-yl]-4*H*-1,2,4-triazol-4-ido}iron(II) methanol disolvate

Kateryna Znovjyak, Maksym Seredyuk, Igor O. Fritsky, Tatiana Y. Sliva, Vladimir M. Amirkhanov, Sergey O. Malinkin and Sergiu Shova

Computing details

Data collection: *CrysAlis PRO* (Rigaku OD, 2022); cell refinement: *CrysAlis PRO* (Rigaku OD, 2022); data reduction: *CrysAlis PRO* (Rigaku OD, 2022); program(s) used to refine structure: *SHELXL2018/3* (Sheldrick, 2015); molecular graphics: Olex2 (Dolomanov *et al.*, 2009); software used to prepare material for publication: Olex2 (Dolomanov *et al.*, 2009).

Bis{3-(3,5-dichlorophenyl)-5-[6-(1*H*-pyrazol-1-yl)pyridin-2-yl]-4*H*-1,2,4-triazol-4-ido}iron(II) methanol disolvate

Crystal data

$[Fe(C_{16}H_9Cl_2N_6)_2]\cdot 2CH_4O$
$M_r = 832.32$
Orthorhombic, *Pnna*
$a = 10.4669$ (6) Å
$b = 26.5890$ (16) Å
$c = 12.8313$ (7) Å
$V = 3571.0$ (4) Å^3
$Z = 4$
$F(000) = 1696$
$D_x = 1.548$ Mg m^{-3}
Mo $K\alpha$ radiation, $\lambda = 0.71073$ Å
Cell parameters from 3167 reflections
$\theta = 2.2$–$25.7°$
$\mu = 0.77$ mm^{-1}
$T = 180$ K
Plate, dark red
0.12 × 0.08 × 0.03 mm

Data collection

Xcalibur, Eos diffractometer
ω scans
Absorption correction: multi-scan (CrysAlisPro; Rigaku OD, 2022)
$T_{min} = 0.772$, $T_{max} = 1.000$
13877 measured reflections
3650 independent reflections
2093 reflections with $I > 2\sigma(I)$
$R_{int} = 0.100$
$\theta_{max} = 26.4°$, $\theta_{min} = 1.8°$
$h = -13\rightarrow 8$
$k = -33\rightarrow 33$
$l = -14\rightarrow 15$
3 standard reflections every 1 reflections
intensity decay: none

Refinement

Refinement on F^2
Least-squares matrix: full
$R[F^2 > 2\sigma(F^2)] = 0.068$
$wR(F^2) = 0.133$
$S = 1.02$
3650 reflections
244 parameters
0 restraints
Primary atom site location: dual
Hydrogen site location: mixed
H atoms treated by a mixture of independent and constrained refinement
$w = 1/[\sigma^2(F_o^2) + (0.0367P)^2]$ where $P = (F_o^2 + 2F_c^2)/3$
$(\Delta/\sigma)_{max} < 0.001$
$\Delta\rho_{max} = 0.44$ e Å^{-3}
$\Delta\rho_{min} = -0.50$ e Å^{-3}

Special details

Geometry. All esds (except the esd in the dihedral angle between two l.s. planes) are estimated using the full covariance matrix. The cell esds are taken into account individually in the estimation of esds in distances, angles and torsion angles; correlations between esds in cell parameters are only used when they are defined by crystal symmetry. An approximate (isotropic) treatment of cell esds is used for estimating esds involving l.s. planes.

Fractional atomic coordinates and isotropic or equivalent isotropic displacement parameters (Å²)

	x	*y*	*z*	U_{iso}*/U_{eq}
C3	0.5057 (4)	0.32367 (15)	0.3495 (3)	0.0204 (10)
C4	0.4305 (4)	0.30235 (16)	0.4341 (3)	0.0207 (10)
C5	0.4296 (4)	0.31360 (16)	0.5392 (3)	0.0261 (11)
H5	0.486168	0.338141	0.566974	0.031*
C6	0.3448 (4)	0.28840 (16)	0.6032 (3)	0.0269 (11)
H6	0.343778	0.295610	0.675694	0.032*
C7	0.2607 (4)	0.25265 (16)	0.5633 (3)	0.0240 (10)
H7	0.201948	0.235235	0.606739	0.029*
C8	0.2672 (4)	0.24384 (15)	0.4571 (3)	0.0203 (10)
C11	0.1361 (4)	0.17150 (16)	0.2626 (3)	0.0278 (11)
H11	0.134864	0.158847	0.193327	0.033*
C12	0.0477 (4)	0.15849 (17)	0.3399 (4)	0.0329 (12)
H12	−0.022909	0.136283	0.332937	0.039*
C13	0.0835 (4)	0.18423 (16)	0.4272 (3)	0.0263 (11)
H13	0.042270	0.183520	0.493174	0.032*
C15	0.6226 (4)	0.36305 (15)	0.2470 (3)	0.0226 (10)
C17	0.7161 (4)	0.39837 (15)	0.2033 (3)	0.0230 (10)
C18	0.7328 (5)	0.40295 (16)	0.0965 (3)	0.0316 (12)
H18	0.680723	0.383994	0.050313	0.038*
C19	0.8241 (5)	0.43469 (18)	0.0572 (4)	0.0406 (14)
C20	0.8995 (5)	0.46402 (18)	0.1219 (4)	0.0379 (13)
H20	0.960900	0.486591	0.093934	0.046*
C21	0.8827 (4)	0.45949 (16)	0.2281 (4)	0.0308 (12)
C22	0.7938 (4)	0.42684 (16)	0.2695 (3)	0.0284 (11)
H22	0.785239	0.423707	0.342916	0.034*
Cl23	0.84640 (18)	0.43743 (7)	−0.07653 (11)	0.0872 (7)
Cl24	0.97624 (13)	0.49547 (5)	0.31098 (11)	0.0546 (4)
Fe1	0.35555 (8)	0.250000	0.250000	0.0188 (2)
N2	0.4852 (3)	0.30368 (12)	0.2542 (2)	0.0181 (8)
N9	0.3518 (3)	0.26658 (12)	0.3953 (2)	0.0186 (8)
N10	0.2211 (3)	0.20353 (12)	0.2984 (3)	0.0205 (8)
N14	0.1893 (3)	0.21100 (12)	0.4017 (3)	0.0211 (9)
N16	0.5911 (3)	0.36088 (13)	0.3493 (3)	0.0222 (9)
N25	0.5611 (3)	0.32899 (13)	0.1872 (2)	0.0211 (9)
C27	0.7592 (6)	0.4265 (2)	0.5709 (4)	0.0617 (18)
H27A	0.843547	0.421309	0.539590	0.093*
H27B	0.768395	0.430711	0.646444	0.093*
H27C	0.719871	0.456689	0.541131	0.093*
O26	0.6821 (4)	0.38493 (13)	0.5506 (3)	0.0541 (12)

H26	0.659 (5)	0.382 (2)	0.485 (4)	0.081*

Atomic displacement parameters (Å²)

	U^{11}	U^{22}	U^{33}	U^{12}	U^{13}	U^{23}
C3	0.024 (3)	0.021 (2)	0.016 (2)	0.001 (2)	−0.001 (2)	−0.0012 (18)
C4	0.019 (3)	0.026 (2)	0.017 (2)	−0.003 (2)	0.002 (2)	−0.001 (2)
C5	0.026 (3)	0.035 (3)	0.018 (2)	−0.005 (2)	−0.002 (2)	0.000 (2)
C6	0.033 (3)	0.034 (3)	0.014 (2)	−0.002 (2)	0.000 (2)	−0.004 (2)
C7	0.024 (3)	0.029 (3)	0.019 (2)	−0.003 (2)	0.004 (2)	−0.002 (2)
C8	0.022 (3)	0.016 (2)	0.023 (2)	0.002 (2)	0.001 (2)	−0.0016 (19)
C11	0.031 (3)	0.026 (2)	0.027 (3)	−0.008 (2)	−0.006 (2)	−0.001 (2)
C12	0.026 (3)	0.036 (3)	0.037 (3)	−0.015 (2)	−0.003 (2)	0.001 (2)
C13	0.019 (3)	0.030 (3)	0.030 (3)	−0.008 (2)	0.003 (2)	0.008 (2)
C15	0.026 (3)	0.018 (2)	0.024 (2)	0.003 (2)	−0.001 (2)	0.006 (2)
C17	0.018 (3)	0.021 (2)	0.030 (3)	0.002 (2)	0.000 (2)	0.000 (2)
C18	0.035 (3)	0.034 (3)	0.026 (3)	−0.013 (2)	0.002 (2)	0.002 (2)
C19	0.047 (4)	0.045 (3)	0.030 (3)	−0.012 (3)	0.010 (3)	0.009 (3)
C20	0.029 (3)	0.038 (3)	0.046 (3)	−0.013 (3)	0.008 (3)	0.011 (3)
C21	0.028 (3)	0.022 (2)	0.043 (3)	−0.004 (2)	0.001 (2)	−0.005 (2)
C22	0.027 (3)	0.027 (3)	0.031 (3)	−0.002 (2)	0.000 (2)	0.005 (2)
Cl23	0.1066 (15)	0.1186 (15)	0.0365 (9)	−0.0712 (13)	0.0153 (10)	0.0100 (9)
Cl24	0.0470 (9)	0.0536 (9)	0.0631 (10)	−0.0229 (8)	−0.0128 (8)	−0.0011 (7)
Fe1	0.0207 (5)	0.0225 (5)	0.0132 (4)	0.000	0.000	−0.0013 (4)
N2	0.019 (2)	0.0223 (18)	0.0134 (18)	0.0009 (16)	0.0027 (17)	0.0002 (16)
N9	0.021 (2)	0.0197 (19)	0.0154 (18)	0.0006 (17)	0.0019 (17)	0.0007 (15)
N10	0.020 (2)	0.022 (2)	0.019 (2)	0.0008 (17)	0.0005 (17)	−0.0017 (16)
N14	0.022 (2)	0.025 (2)	0.016 (2)	−0.0007 (18)	0.0035 (17)	0.0010 (16)
N16	0.022 (2)	0.027 (2)	0.017 (2)	−0.0023 (18)	0.0021 (17)	0.0025 (17)
N25	0.023 (2)	0.022 (2)	0.019 (2)	0.0022 (18)	0.0059 (17)	0.0041 (16)
C27	0.071 (5)	0.062 (4)	0.053 (4)	−0.024 (4)	−0.001 (3)	−0.019 (3)
O26	0.073 (3)	0.059 (3)	0.030 (2)	−0.036 (2)	−0.008 (2)	0.001 (2)

Geometric parameters (Å, º)

C3—C4	1.456 (5)	C17—C22	1.398 (6)
C3—N2	1.351 (5)	C18—H18	0.9500
C3—N16	1.333 (5)	C18—C19	1.371 (6)
C4—C5	1.382 (5)	C19—C20	1.386 (6)
C4—N9	1.353 (5)	C19—Cl23	1.733 (5)
C5—H5	0.9500	C20—H20	0.9500
C5—C6	1.383 (6)	C20—C21	1.379 (6)
C6—H6	0.9500	C21—C22	1.380 (6)
C6—C7	1.393 (5)	C21—Cl24	1.733 (5)
C7—H7	0.9500	C22—H22	0.9500
C7—C8	1.385 (5)	Fe1—N2	1.970 (3)
C8—N9	1.334 (5)	Fe1—N2^{i}	1.970 (3)
C8—N14	1.391 (5)	Fe1—N9^{i}	1.916 (3)

C11—H11	0.9500	Fe1—N9	1.916 (3)
C11—C12	1.400 (6)	Fe1—N10^{i}	1.973 (3)
C11—N10	1.315 (5)	Fe1—N10	1.973 (3)
C12—H12	0.9500	N2—N25	1.350 (4)
C12—C13	1.366 (6)	N10—N14	1.381 (4)
C13—H13	0.9500	C27—H27A	0.9800
C13—N14	1.357 (5)	C27—H27B	0.9800
C15—C17	1.468 (6)	C27—H27C	0.9800
C15—N16	1.355 (5)	C27—O26	1.393 (6)
C15—N25	1.350 (5)	O26—H26	0.88 (5)
C17—C18	1.387 (5)		

N2—C3—C4	115.8 (4)	C20—C21—C22	121.4 (4)
N16—C3—C4	130.8 (4)	C20—C21—Cl24	119.1 (4)
N16—C3—N2	113.4 (4)	C22—C21—Cl24	119.5 (4)
C5—C4—C3	130.3 (4)	C17—C22—H22	120.0
N9—C4—C3	109.2 (3)	C21—C22—C17	119.9 (4)
N9—C4—C5	120.5 (4)	C21—C22—H22	120.0
C4—C5—H5	120.7	N2^{i}—Fe1—N2	92.94 (18)
C4—C5—C6	118.6 (4)	N2^{i}—Fe1—N10	92.64 (13)
C6—C5—H5	120.7	N2^{i}—Fe1—N10^{i}	159.46 (13)
C5—C6—H6	119.4	N2—Fe1—N10^{i}	92.64 (13)
C5—C6—C7	121.3 (4)	N2—Fe1—N10	159.46 (13)
C7—C6—H6	119.4	N9^{i}—Fe1—N2^{i}	79.69 (14)
C6—C7—H7	121.8	N9^{i}—Fe1—N2	101.95 (13)
C8—C7—C6	116.5 (4)	N9—Fe1—N2	79.68 (14)
C8—C7—H7	121.8	N9—Fe1—N2^{i}	101.95 (13)
C7—C8—N14	125.5 (4)	N9^{i}—Fe1—N9	177.7 (2)
N9—C8—C7	122.8 (4)	N9^{i}—Fe1—N10^{i}	79.82 (14)
N9—C8—N14	111.7 (3)	N9^{i}—Fe1—N10	98.49 (14)
C12—C11—H11	124.5	N9—Fe1—N10	79.82 (14)
N10—C11—H11	124.5	N9—Fe1—N10^{i}	98.49 (14)
N10—C11—C12	111.1 (4)	N10^{i}—Fe1—N10	89.01 (19)
C11—C12—H12	127.0	C3—N2—Fe1	114.8 (3)
C13—C12—C11	106.0 (4)	N25—N2—C3	106.6 (3)
C13—C12—H12	127.0	N25—N2—Fe1	138.5 (3)
C12—C13—H13	126.6	C4—N9—Fe1	120.5 (3)
N14—C13—C12	106.8 (4)	C8—N9—C4	120.3 (3)
N14—C13—H13	126.6	C8—N9—Fe1	119.2 (3)
N16—C15—C17	124.0 (4)	C11—N10—Fe1	141.1 (3)
N25—C15—C17	122.0 (4)	C11—N10—N14	105.4 (3)
N25—C15—N16	114.0 (4)	N14—N10—Fe1	112.6 (2)
C18—C17—C15	121.2 (4)	C13—N14—C8	133.2 (4)
C18—C17—C22	118.6 (4)	C13—N14—N10	110.7 (3)
C22—C17—C15	120.2 (4)	N10—N14—C8	116.1 (3)
C17—C18—H18	119.8	C3—N16—C15	101.3 (3)
C19—C18—C17	120.4 (4)	N2—N25—C15	104.7 (3)
C19—C18—H18	119.8	H27A—C27—H27B	109.5

C18—C19—C20	121.5 (4)	H27A—C27—H27C	109.5
C18—C19—Cl23	119.0 (4)	H27B—C27—H27C	109.5
C20—C19—Cl23	119.6 (4)	O26—C27—H27A	109.5
C19—C20—H20	121.0	O26—C27—H27B	109.5
C21—C20—C19	118.1 (4)	O26—C27—H27C	109.5
C21—C20—H20	121.0	C27—O26—H26	114 (4)
C3—C4—C5—C6	178.0 (4)	C18—C17—C22—C21	1.4 (7)
C3—C4—N9—C8	−175.6 (3)	C18—C19—C20—C21	1.7 (8)
C3—C4—N9—Fe1	1.7 (5)	C19—C20—C21—C22	0.0 (7)
C3—N2—N25—C15	−0.3 (4)	C19—C20—C21—Cl24	179.7 (4)
C4—C3—N2—Fe1	0.6 (5)	C20—C21—C22—C17	−1.5 (7)
C4—C3—N2—N25	178.7 (3)	C22—C17—C18—C19	0.2 (7)
C4—C3—N16—C15	−178.2 (4)	Cl23—C19—C20—C21	−177.5 (4)
C4—C5—C6—C7	−0.5 (7)	Cl24—C21—C22—C17	178.8 (3)
C5—C4—N9—C8	3.9 (6)	Fe1—N2—N25—C15	177.2 (3)
C5—C4—N9—Fe1	−178.7 (3)	Fe1—N10—N14—C8	−8.8 (4)
C5—C6—C7—C8	0.2 (6)	Fe1—N10—N14—C13	170.2 (3)
C6—C7—C8—N9	2.3 (6)	N2—C3—C4—C5	179.1 (4)
C6—C7—C8—N14	−177.8 (4)	N2—C3—C4—N9	−1.4 (5)
C7—C8—N9—C4	−4.4 (6)	N2—C3—N16—C15	0.2 (4)
C7—C8—N9—Fe1	178.2 (3)	N9—C4—C5—C6	−1.5 (6)
C7—C8—N14—C13	8.4 (7)	N9—C8—N14—C13	−171.8 (4)
C7—C8—N14—N10	−173.0 (4)	N9—C8—N14—N10	6.9 (5)
C11—C12—C13—N14	−0.3 (5)	N10—C11—C12—C13	−0.5 (5)
C11—N10—N14—C8	179.7 (3)	N14—C8—N9—C4	175.7 (3)
C11—N10—N14—C13	−1.3 (4)	N14—C8—N9—Fe1	−1.7 (5)
C12—C11—N10—Fe1	−166.3 (3)	N16—C3—C4—C5	−2.5 (8)
C12—C11—N10—N14	1.1 (5)	N16—C3—C4—N9	177.0 (4)
C12—C13—N14—C8	179.7 (4)	N16—C3—N2—Fe1	−178.1 (3)
C12—C13—N14—N10	1.0 (5)	N16—C3—N2—N25	0.1 (5)
C15—C17—C18—C19	−177.5 (4)	N16—C15—C17—C18	−172.0 (4)
C15—C17—C22—C21	179.1 (4)	N16—C15—C17—C22	10.3 (6)
C17—C15—N16—C3	−179.5 (4)	N16—C15—N25—N2	0.5 (5)
C17—C15—N25—N2	179.6 (3)	N25—C15—C17—C18	8.9 (6)
C17—C18—C19—C20	−1.8 (8)	N25—C15—C17—C22	−168.7 (4)
C17—C18—C19—Cl23	177.4 (4)	N25—C15—N16—C3	−0.4 (4)

Symmetry code: (i) x, $-y+1/2$, $-z+1/2$.

Hydrogen-bond geometry (Å, º)

D—H···*A*	*D*—H	H···*A*	*D*···*A*	*D*—H···*A*
C5—H5···O26	0.95	2.41	3.256 (6)	149
C7—H7···N25^{ii}	0.95	2.48	3.406 (5)	165
C11—H11···O26^{iii}	0.95	2.23	3.144 (6)	162
C13—H13···N25^{ii}	0.95	2.52	3.363 (6)	148

C20—H20···Cl23^{iv}	0.95	2.86	3.779 (5)	162
O26—H26···N16	0.88 (5)	1.96 (5)	2.826 (5)	166 (5)

Symmetry codes: (ii) $x-1/2, -y+1/2, z+1/2$; (iii) $x-1/2, -y+1/2, z-1/2$; (iv) $-x+2, -y+1, -z$.